Electrical Engineering   School of Engineering

11-26-1990

Characterization of SiGe/Si Heterostructures Formed by Ge+ and C+ Implantation

Akira Fukami

Ken-Ichi Shoji

Takahiro Nagano

Cary Y. Yang
Santa Clara University, cyang@scu.edu

Characterization of SiGe/Si heterostructures formed by Ge+ and C+ implantation

Akira Fukami, Ken-ichi Shoji, and Takahiro Nagano
Hitachi Research Laboratory, Hitachi, Ltd., 4026 Kuji, Hitachi, Ibaraki 319-12, Japan

Cary Y. Yang
Microelectronics Laboratory, Santa Clara University, Santa Clara, California 95053

Formation of SiGe/Si heterostructures by germanium ion implantation was investigated. A germanium-implanted layer was grown epitaxially in the solid phase by thermal annealing. Two kinds of crystalline defects were observed. One is a misfit dislocation, and the other is a residual dislocation caused by ion bombardment. The *p-n* junction formed in the SiGe layer has a leakage current three orders of magnitude larger than that of a pure Si *p-n* junction fabricated with an identical process except for the Ge+ implantation. Carbon doping in the SiGe layer improves its crystalline quality and the junction characteristics.

Recently, studies on the fabrication of SiGe/Si heterojunction bipolar transistors with various techniques have been reported.[1-5] For example, deposition of SiGe with molecular beam epitaxy (MBE) can optimize control of impurity profiles.[1] However, considering the compatibility with current silicon integrated circuit fabrication lines, it would be difficult and extremely costly to merge anyone of these techniques with a standard process. Ion implantation is a technique highly compatible with any standard silicon process, and has been shown to be suitable for fabricating SiGe alloys.[6-12] In this study, SiGe/Si heterostructures are fabricated using germanium ion implantation into silicon and subsequent solid phase epitaxy (SPE). Microstructure of the implanted layer as well as electrical characteristics of *p-n* diodes formed is examined. A technique for improving the crystalline quality of the SiGe layer is suggested. Instead of using boron as reported previously,[12] carbon ion implant is added to the process. Being isoelectronic with Si and Ge, C is not a dopant and is more likely to reduce the lattice strain introduced by Ge. Our results show improvements in both crystallinity and junction properties.

Germanium ions were implanted into *n*-type Si(100) through a thermally grown 10 nm oxide at an acceleration energy of 50 keV with a dose of 2.5×10^{16} cm^{-2}. The peak germanium concentration is about 8×10^{21} cm^{-3}. This value corresponds to a germanium content of 16 at.%. For some samples, carbon ion implantation was subsequently carried out to compensate for the lattice mismatch between the silicon substrate and the implanted layer. Carbon ions were implanted at an energy of 15 keV with a dose of 3×10^{15} cm^{-2}. This energy was chosen to yield equal projected ranges for both germanium and carbon ions. The carbon dosage was determined to provide an average lattice constant for the Si-Ge-C mixture equal to that of Si. These samples were then furnace-annealed in a N$_2$ ambient at 600 °C for 24 h. Rapid thermal annealing (RTA) at 1000 °C for 10 s was also performed on some samples.

In order to evaluate the crystalline quality electrically, a planar *p-n* junction structure was utilized. Figure 1 shows a schematic of the device geometry. Germanium ions were implanted into *p*-type Si(100) at an acceleration energy of

120 keV with a dose of 5×10^{16} cm^{-2}. For some samples, carbon ions were subsequently implanted at 33 keV with a dose range of $3-12.5 \times 10^{15}$ cm^{-2}. Boron ion implant then followed to form the p^+ region. Thus the diode formed is not a heterojunction, merely one with a varying but continuous band gap across the device. Two annealing steps were carried out. First, a low-temperature anneal occurred at 600 °C for 24 h, followed by one at 950 °C for 10 min. The latter is equivalent to the RTA performed for the TEM samples and is part of a standard bipolar process. Then, a SiO$_2$ overlayer was added, diffusion windows were opened, and a poly-Si film was deposited. Arsenic and boron ions were implanted to form the n^{++} and p^{++} regions respectively. A furnace anneal at 950 °C for 10 min was then performed. Finally, aluminum deposition was made to form metal contacts.

Figure 2 shows the germanium concentration profiles for samples as-implanted and after annealing, with the dotted curve indicating the simulation result. The as-implanted result shows a higher concentration at the surface and a deeper penetration than those of the simulation. These differences are attributed to diffusion during ion implantation as a result of beam heating. Upon annealing at 600 °C for 24 h, germanium ions diffused about 25 nm further into the substrate.

Cross-sectional transmission electron micrographs (XTEMs) of an as-implanted sample and an annealed sample are shown in Fig. 3. Figure 3(a) shows the interface between the amorphized layer and the silicon substrate in the as-implanted sample, as viewed from a ⟨110⟩
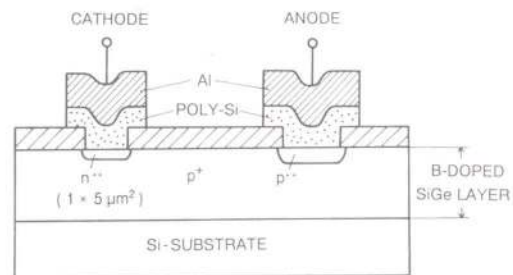

FIG. 1. Schematic cross section of a SiGe n^{++}-p^+ junction.
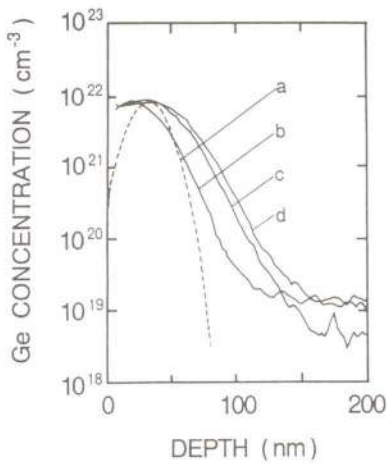
FIG. 2. SIMS profiles of Ge in Si: (a) as-implanted (simulation), (b) as-implanted (experiment), (c) annealed at 600 °C for 24 h, (d) same as (c) followed by RTA at 1000 °C for 10 s.

direction. The implanted region is totally amorphized. In the silicon substrate there are some strains and defects caused by the germanium ion implantation. Figure 3(b) shows the interface between the recrystallized layer and the substrate in the furnace-annealed sample. It contains dislocations due to residual germanium ion damage. The lattice image shows that the SiGe layer is epitaxially regrown on the silicon substrate. Figure 3(c) is another high-resolution micrograph for the furnace-annealed sample, showing the surface region. The lattice image reveals that the top layer is still amorphous even after annealing at 600 °C for 24 h. The existence of this amorphous layer is due to a low SPE rate, probably caused by the presence of oxygen from the oxide layer. It also shows that the interface between the amorphous and recrystallized SPE layers contains many line and planar defects forming an angle of about 60° with the surface. Similar features were observed in MBE-grown SiGe/Si heterostructures[13] and SPE-regrown SiGe alloys.[11] In view of the high Ge concentration in this region, these defects are attributed to misfit dislocations associated with growth of the SPE layer.

Figure 4 shows two XTEM images for a sample implanted with Ge$^+$ and one implanted with both Ge$^+$ and C$^+$. There is little change in the defects of the interface region due to carbon doping. However, the defects near the surface are reduced considerably by the presence of carbon.

Figure 5 summarizes results of room-temperature current-voltage measurements for three diodes. A comparison of forward current-voltage characteristics is shown in Fig. 5(a). The vertical axis shows the current density in the n^{++} region. Both the SiGe and the carbon-doped SiGe diodes exhibit larger currents and smaller slopes than the Si diode. This is attributed to carrier recombination associated with defects near the SiGe surface. These defects give rise to recombination/generation centers throughout the diode. The forward current decreases as carbon ions are added. However, the slope does not change appreciably. This parallel downward shift corresponds to an increase of about 0.06 eV in band gap due to carbon doping. This increase in band gap is approximately the same as the
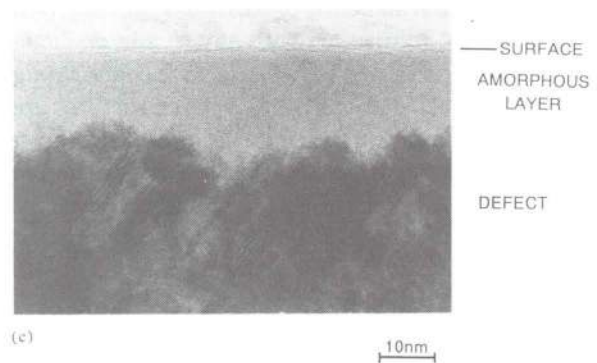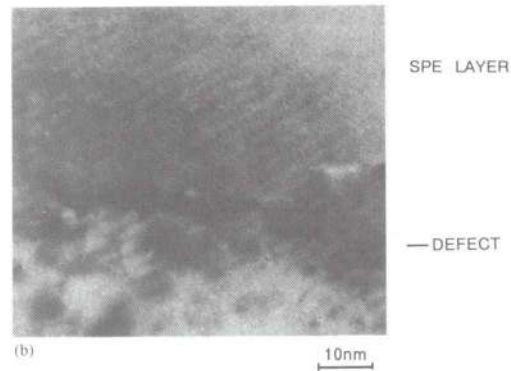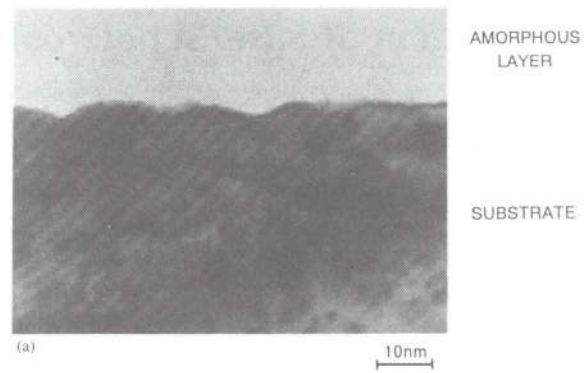

FIG. 3. High-resolution XTEM images of SiGe/Si: (a) interface between amorphous layer and substrate of as-implanted sample, (b) interface between recrystallized layer and substrate of sample annealed at 600 °C for 24 h, (c) subsurface region of sample in (b).

estimated value based on Ge and C concentrations near the junctions. The reverse characteristics are displayed in Fig. 5(b). The leakage current of the SiGe diode is about six times larger than that of the SiGe:C diode and about three orders of magnitude larger than that of a pure Si diode. As in the forward-bias case, this is due to band-gap differences as well as larger generation current associated with defects in the SiGe layer. Aside from band-gap effect, the decrease in leakage current as a result of carbon doping can also be attributed to improvement in crystalline quality. Figure 5(c) shows the dependence of the breakdown voltage on the carbon ion dose. As a reference, the values for the SiGe diode and the pure Si diode are also plotted. The SiGe diode has the lowest breakdown voltage. However, the breakdown voltage increases with an increase in carbon ion dose, further confirming the improvement in crystalline quality due to carbon doping.
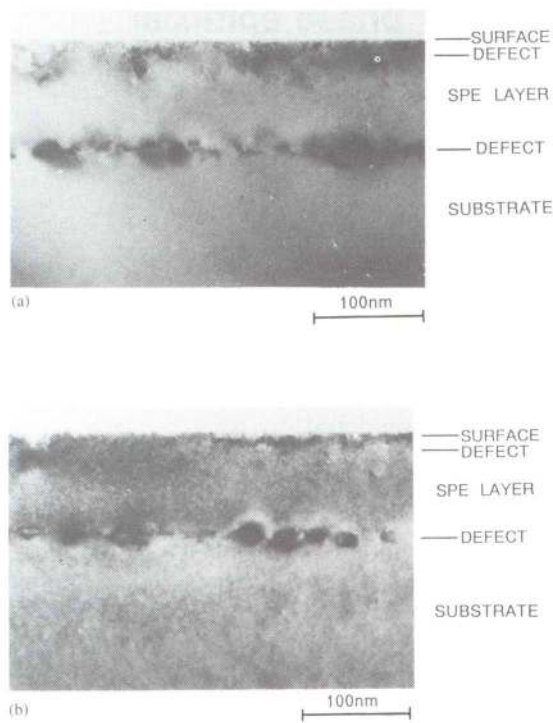
FIG. 4. XTEM images of SiGe/Si heterostructures annealed at 600 °C for 24 h followed by RTA at 1000 °C for 10 s: (a) without carbon doping, (b) with a C^+ dose of 3×10^{15} cm^{-2}.
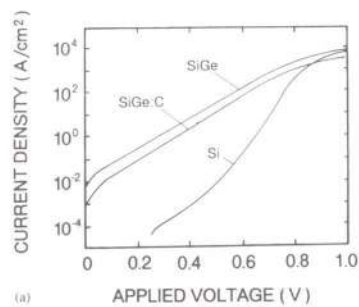
To summarize, SiGe heterostructures were formed by germanium ion implantation followed by thermal annealing. There are two kinds of defects in the recrystallized SiGe layer. One is a misfit dislocation due to the high content of germanium, which makes an angle of 60° with the surface. The other is a residual dislocation at the recrystallized-layer/substrate interface. The addition of carbon has little effect on the defects at this interface, but reduces the surface defects substantially. *p-n* junctions were fabricated in the SiGe layer. The forward current is larger than that of a pure Si diode and is attributed to additional recombination centers across the diode. The reverse leakage current decreases while the breakdown voltage increases with increasing C^+ dose. Thus, carbon doping improves the SiGe crystalline quality and consequently the diode properties.

FIG. 5. Comparisons of diode current-voltage characteristics: (a) forward bias, (b) reverse bias. The C^+ dose in the SiGe:C diode is 1.25×10^{16} cm^{-3}. (c) shows the dependence of reverse-bias breakdown voltage on C^+ dose.
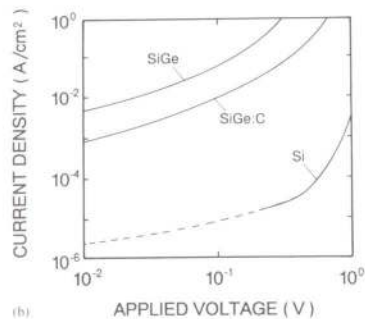
[1] G. L. Patton, S. S. Iyer, S. L. Delage, S. Tiwari, and J. M. C. Stork, IEEE Electron. Device Lett. **9**, 165 (1988).

[2] D. Xu, G. Shen, M. Willander, W. Ni, and G. V. Hansson, Appl. Phys. Lett. **52**, 2239 (1988).
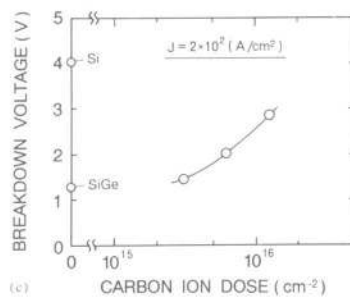
[3] H.-U. Schreiber and B. G. Bosch, IEDM Tech. Dig., 643 (1989).

[4] T. T. Kamins, K. Nauka, L. H. Camnitz, J. B. Kruger, J. E. Turner, S. J. Rosner, M. P. Scott, J. L. Hoyt, C. A. King, D. B. Noble, and J. F. Gibbons, IEDM Tech. Dig., 647 (1989).

[5] S. E. Fischer, R. K. Cook, R. W. Knepper, R. C. Range, K. Nummy, D. C. Ahlgren, M. Revitz, and B. S. Meyerson, IEDM Tech. Dig., 890 (1989).

[6] R. R. Hart, R. G. Hunsperger, H. L. Dunlap, and O. J. Marsh, Nucl. Instrum. Methods **190**, 70 (1981).

[7] O. W. Holland, C. W. White, and D. Fathy, Appl. Phys. Lett. **51**, 520 (1987).

[8] D. Fathy, O. W. Holland, and C. W. White, Appl. Phys. Lett. **51**, 1337 (1987).

[9] J. Narayan, S. Sharan, A. R. Srivatsa, and A. S. Nandedka, Mater. Sci. Eng. B 1, 105 (1988).

[10] A. R. Srivatsa, S. Sharan, O. W. Holland, and J. Narayan, J. Appl. Phys. **65**, 4028 (1989).

[11] D. C. Paine, D. J. Howard, N. G. Stoffel, and J. A. Horton, J. Mater. Res. **5**, 1023 (1990).

[12] K. Ohta, J. Sakano, and S. Furukawa, Extended Abstracts of 21st Conf. Solid State Devices and Materials, Tokyo, 1989, p. 555.

[13] Y. Fukuda, Y. Kohama, M. Seki, and Y. Ohmachi, Jpn. J. Appl. Phys. **28**, L19 (1989).